

Partial Discharge Characterization of Ceramic Power Electronics Circuit Carriers Assisted by Machine Learning

Johannes Drechsel

Systems Integration and Electronic Packaging

Fraunhofer Institute for Ceramic Technologies and Systems IKTS

Dresden, Germany

johannes.drechsel@ikts.fraunhofer.de

Henry Barth

Systems Integration and Electronic Packaging

Fraunhofer Institute for Ceramic Technologies and Systems IKTS

Dresden, Germany

henry.barth@ikts.fraunhofer.de

Lars Rebenklau

Systems Integration and Electronic Packaging

Fraunhofer Institute for Ceramic Technologies and Systems IKTS

Dresden, Germany

lars.rebenklau@ikts.fraunhofer.de

Abstract— This paper presents an approach for transferring knowledge about partial discharges in polymer insulators to ceramic insulators with the aid of machine learning. It is shown how various machine-learnable features can be generated from partial discharge measurement data and processed in varying artificial neural networks for classification. It is found that polymer-based partial discharges can be classified using this method. In addition, the Long Short-Term Memory based artificial neural network enables partial discharge cause finding and thus fault detection in ceramic power electronics substrates.

Keywords—Ceramics, Partial Discharges, Machine Learning, High Voltage, High Frequency

I. INTRODUCTION

Electronics are used in almost all areas of life, whereby the electronic assemblies are usually mounted on rigid carriers. The common green fiberglass composite boards, for example in PCs or smartphones, are well known in this context. This material, called FR-4, is used extensively in the consumer sector. Here, the requirements on thermomechanical, chemical, and electrical stability are comparatively low while cost pressure is high. The situation is different for high-voltage switchgear or power electronics assemblies, widely used in the e-mobility sector. Here, ceramic carrier boards are used due to the increased requirements. These include higher operating voltage, circuit waste heat, and harsh environmental conditions in an often limited package size. Despite the excellent material properties of ceramics, certain high-voltage systems are based on polymer insulators. Operation of these systems has shown repeatedly that the occurrence of so-called partial discharges (PD) can impair their insulation properties. Over time, this phenomenon can lead to an electrical breakdown and thus total failure of the system. Therefore, close monitoring is necessary, which places high voltage and frequency requirements on the measurement technology due to the PD-inherent occurrence characteristics. Furthermore, vast amounts of data are recorded during PD measurements, which must be processed, visualized, and interpreted. To address these matters, this work evaluates the following points:

- Knowledge transfer from polymer-based insulation systems to ceramics
- Use of machine learning in ceramics-based PD classification

II. PARTIAL DISCHARGES

A. Occurrence

The phenomenon of failing insulation is commonly known in the form of lightning during a thunderstorm. Simply put, the trigger for such a breakdown is the potential difference between the high voltage side and ground, which allows a starting electron to build up enough kinetic energy to carry other electrons along in an avalanche effect. This leads to the formation of a conduction channel in the previously poorly conducting medium, which transports electrical charge. So, concluding, the electric field strength must exceed the breakdown limit of the insulation material for a discharge to occur. Scaled down, this means that discharges can also occur in partial regions of the insulator as long as the maximum local intrinsic field strength is exceeded and a start electron is available. The discharges occurring in a part of the total insulator are consequently called partial discharges. Despite the local confinement, these, as well as complete breakdowns, can damage the insulator by means of heat emission, vibrations, photons or chemically.

B. Model

For a better understanding of this behavior in solid insulators such as ceramics, the capacitive equivalent circuit for partial discharges by Philippoff and Gemant (Fig. 1) is used.

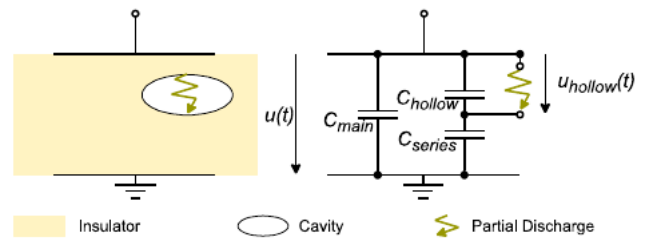


Fig. 1. Capacitive PD model view [1].

In this model conception, it is assumed that both the ideal insulation path (C_{main}) and possible imperfections (C_{hollow}) as well as the surrounding, undisturbed insulation material (C_{series}) are described as capacitors. The PDs that occur when an alternating voltage of sufficient amplitude is applied are represented by the spark gap. Inherent in both the model and the real test specimen is that the transported charge (q_{real}) cannot be measured directly but can be described in relation to the charge measured at the substrate (q_{app}) by (1) [2].

$$q_{\text{real}} = q_{\text{app}} * \frac{C_{\text{hollow}} + C_{\text{series}}}{C_{\text{series}}} \quad (1)$$

C. Measurement

The measurement setup shown schematically in Fig. 2 is suitable for inducing and measuring partial discharges.

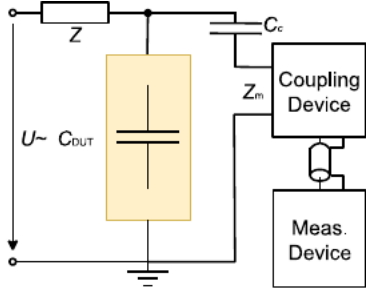


Fig. 2. PD measurement setup schematic conforming to IEC 60270 [3].

In order to be able to determine the apparently transported charge q_{app} , the measuring device must be calibrated to the entire setup including the test specimen. This is done using pulses of known amplitude applied directly to the device under test without applying the test voltage. Just like the PDs induced in the test setup when a high voltage is applied, these pulses manifest themselves as high-frequency current spikes in the supply line. To determine this charge quantitatively, the high-frequency high-voltage PD signal is decoupled via coupling capacitors (C_c) as well as filters and calculated from voltage peaks across the measuring impedance Z_m according to (2).

$$q_{app} = \int_{t_1}^{t_2} i(t) dt = \frac{1}{Z_m} \int_{t_1}^{t_2} u(t) dt \quad (2)$$

A real-time measurement device that implements both peak detection and integration is shown schematically in Fig. 3.

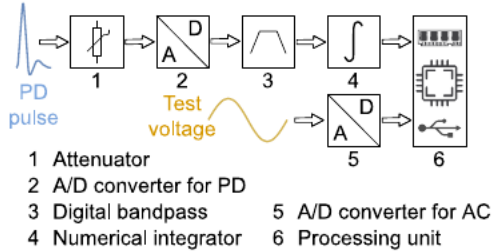


Fig. 3. Real-time PD measuring device schematic conforming to [3].

In addition, such a device detects the alternating test voltage and sets the time of occurrence of each PD in phase relation to it. Thus, the measuring device provides the following data triplet for each PD:

- Apparent charge
- Time of occurrence
- Phase

D. Data Evaluation

In order to gain insights into the partial discharge origins from the generated data (up to several million events per second), two visualization methods have been established. One is an amplitude-phase correlation called phase resolved partial discharge pattern (PRPD, Fig. 4), the other is the correlation of successive pulses, called pulse sequence analysis (PSA, Fig. 5).

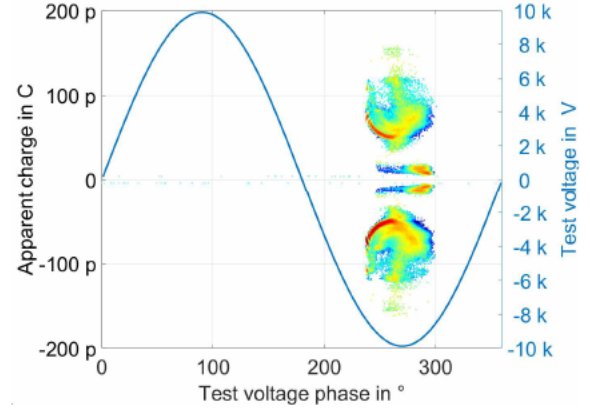


Fig. 4. Exemplary PRPD.

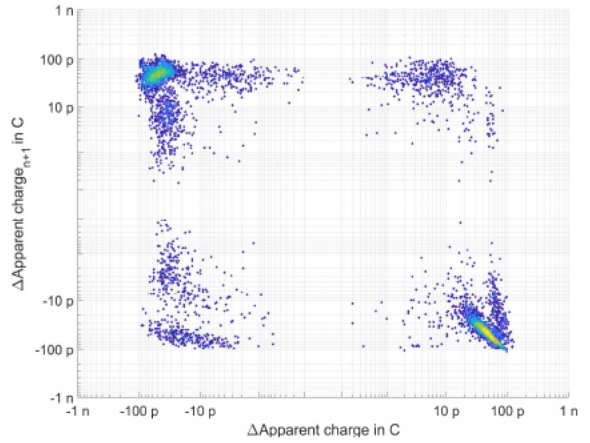


Fig. 5. Exemplary PSA.

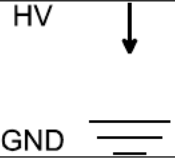
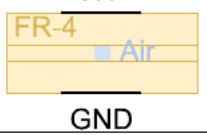
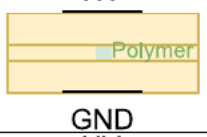
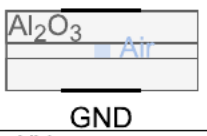
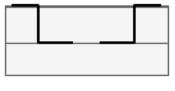
Established PD literature states that the patterns shown exhibit significant differences depending on the PD origin (e.g., point-plate structure, cavity discharge, surface-gliding discharge) [4, 5]. Since classifying millions of pulse shapes by hand is impractical, some form of machine pattern recognition must be employed.

III. APPROACH

A. Test Specimens

To enable knowledge transfer from PDs in gaseous and polymer insulators to PDs in ceramic circuit carrier boards, the test specimens shown in Tab. I are used.

TABLE I. TEST SEPCIMENS

No.	Description	Schematic	Expected PD types
1	Point-plate in air		Corona discharges
2	Cavity in FR-4		Cavity discharges, external corona discharges
3	Inclusion in FR-4		Cavity discharges, boundary layer discharges, external corona discharges
4	Cavity in ceramic		Cavity discharges, external corona discharges
5	Point-point in ceramic		Cavity discharges, boundary layer discharges, external corona discharges

The use of comparatively easy-to-manufacture polymer substrates with defined inclusions enables precise knowledge about the main PD origins in each measurement. This allows for their labeling for the subsequent machine learning. The need for manual labeling arises from the use of supervised learning approaches in Section III D. These approaches require predefined classes for each sample in order to learn the dependency between label and input data in the training process.

B. Partial Discharge Source Differentiation

In real applications, depending on the type and number of superimposed PD origins, differentiation between origins is difficult. This makes a meaningful PSA impossible, since actually independent PDs are set in relation to each other due to their temporal position. Consequently, an in-depth understanding of possible PD sources remains difficult. Therefore, the individual pulse shapes are used for clustering in literature [6, 7]. Fig. 6 shows data from air and polymer measurements in two possible planes. The purpose here is to show the usual overlapping within the planes, the Time/Bandwidth map is explained in more detail in the following section.

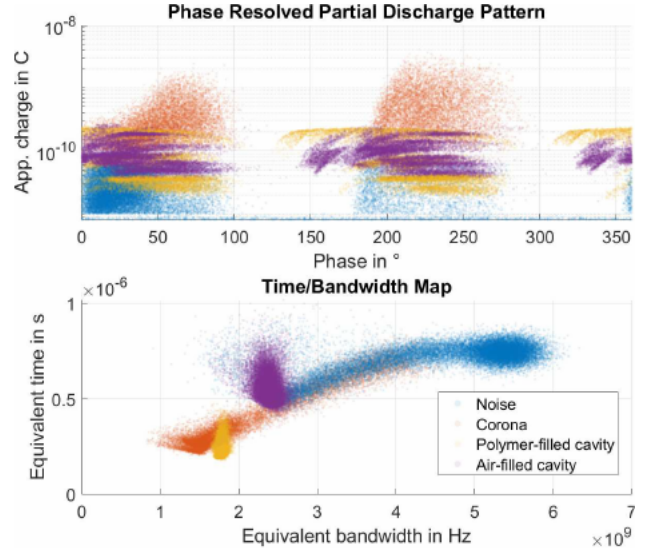


Fig. 6. Data from 4 different sources as PRPD and T/W map.

C. Feature Extraction

Since the standardized measuring device used only supplies data triplets, a transient recorder sampling at 100 MSamples/s is triggered for 10 s as soon as a PD level of 25 pC is reached. As the trigger time is influenced by operating system and communication delays, recorded data are synchronized according to Fig. 7.

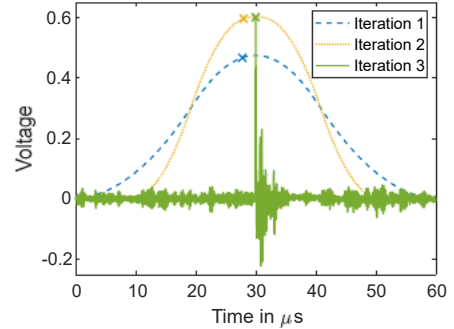


Fig. 7. Synchronization algorithm.

The synchronization algorithm shifts the most prominent time-charge samples in three steps:

- Shift over minimum-maximum-filtered raw data between -0.01 s ... 0.65 s in 400 ns steps
- Shift over minimum-maximum-filtered raw data between -0.065 s ... 0.065 s in 200 ns steps
- Shift over raw data between -0.013 s ... 0.013 s in 10 ns steps

The time-charge samples are shifted by a time determined from the maximum of the summed raw data values at each shift step following each iteration. This approach achieves high precision with comparatively low computation time due to the multi-step method.

As the overlap in the two usual charge-phase and time-bandwidth planes is still significant, additional features have to be calculated. From the extracted single pulses, the features shown in Tab. II are calculated with $s(t)$ being the signal in time domain, $\tilde{S}(f)$ being the signal in frequency domain and $A(i)$ being the signal sampled at N discrete times.

TABLE II. CALCULATED FEATURES

Marker	Name	Equation
	Normalized signal (helper) [6]	$\tilde{s}(t) = \frac{s(t)}{\sqrt{\int_0^T s(t)^2 dt}}$
	Gravity center (helper) [6]	$t_0 = \int_0^T t \tilde{s}(t)^2 dt$
✕	Equivalent time [6]	$\sigma_T = \sqrt{\int_0^T (t - t_0)^2 \tilde{s}(t)^2 dt}$
—	Equivalent bandwidth [6]	$\sigma_F = \sqrt{\int_0^\infty f^2 \tilde{S}(f) ^2 df}$
	Mean (helper)	$\mu = \frac{1}{N} \sum_{i=1}^N A_i$
	Standard deviation (helper)	$S = \sqrt{\frac{1}{N-1} \sum_{i=1}^N A_i - \mu ^2}$
◇	Equivalent wave	$\sigma_W = \frac{\sigma_F}{S}$
●	Mean steepness	$\mu_\Delta = \frac{1}{N} \sum_{i=1}^N \Delta A_i $
△	Overshoot	$\hat{D} = \frac{ A_{min} }{ A_{max} }$ for $ A_{min} < A_{max} $ $\hat{D} = \frac{ A_{max} }{ A_{min} }$ for $ A_{min} > A_{max} $
▷	Equivalent pulselength	$\sigma_T = \frac{\sum_{i=1}^N A_i - A_{min}}{N}$

To visualize these features, Fig. 8 shows three differently shaped pulses as well as their normalized features.

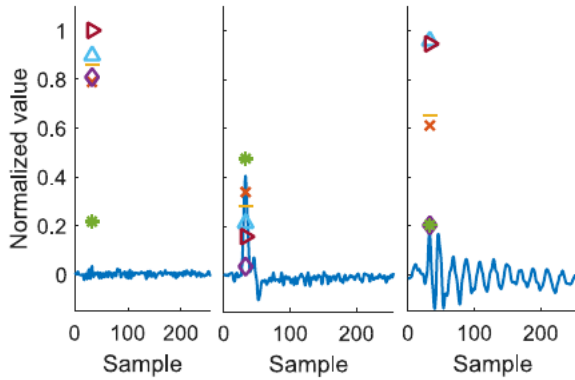


Fig. 8. Exemplary pulse shapes and their normalized features.

It is worth noting that the significance of the extracted features depends on the signal-to-noise ratio and the length of the time series evaluated per pulse [7].

To illustrate this, Fig. 9 and Fig. 10 show Time/Bandwidth maps of 4 different measurements calculated from time series lengths of 2.56 μ s and 10.24 μ s, respectively.

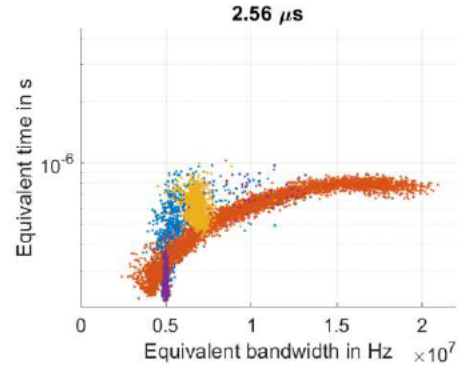


Fig. 9. Time/Bandwidth map using 2.56 μ s extraction length.

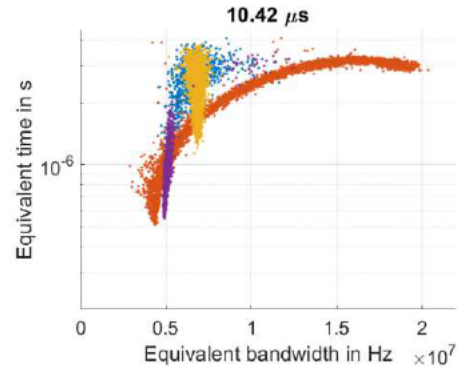


Fig. 10. Time/Bandwidth map using 10.42 μ s extraction length.

It is shown that the selection of an appropriate evaluation length reduces the dispersion of the data within each cluster and thus enables a better separation between the clusters.

To enable evaluation of different machine learning techniques, the time series of each pulse is extracted (Fig. 11).

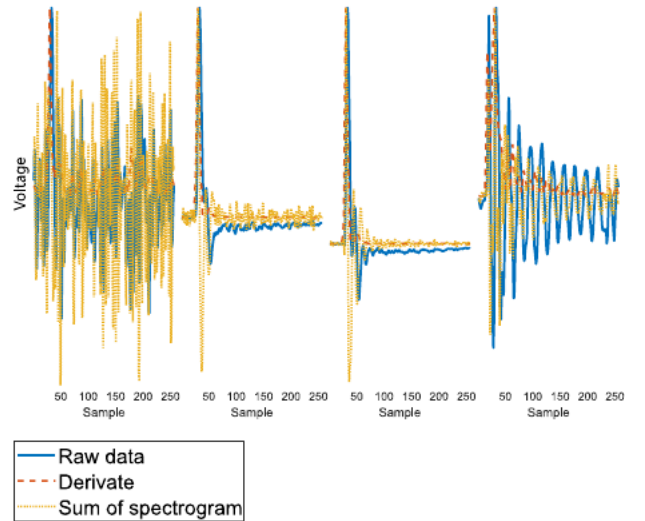


Fig. 11. Extracted time series of noise, corona discharge, filled cavity discharge and polymer-filled discharge (left to right).

Finally, a 192x192 pixel image consisting of the spectrogram superimposed with the pulse shape is generated for each discharge (Fig. 12).

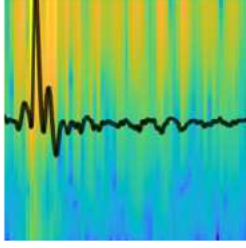


Fig. 12. Image input generated from spectrogram and pulse shape.

D. Machine Learning

The machine learning implementation must accomplish two tasks:

- Learn classification from air- and polymer-based measurements
- Classify samples acquired using ceramic substrates

For this purpose, the polymer- and air-based measurement data are manually labeled as four classes shown in Tab. III.

TABLE III. LABEL OVERVIEW

Name	Origin	Pulse Shape
Noise	Test setup	
Corona in air	Test setup	
External corona	Substrate metallization	
Cavity	Gas-filled cavities inside substrate	

No clear class could be established for gliding boundary layer discharges. This could be due to their non-occurrence or lack of differentiability from external corona discharges. The following three approaches are trained using these data.

1) Multilayer Perceptron (MLP)

In this network of fully connected layers, only the features are processed at each iteration, which makes it resource-efficient and thus fast (Fig. 13).

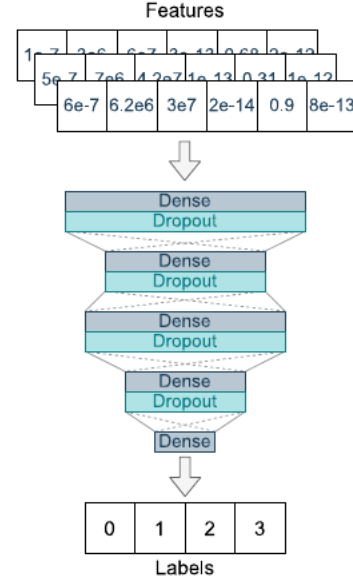


Fig. 13. Fully connected Multilayer Perceptron schematic.

2) Long Short-Term Memory Network

This type of network consists of a block of Long Short-Term Memory (LSTM) cells which enable learning of long-term dependencies as well as a stack of fully connected layers (Fig. 14).

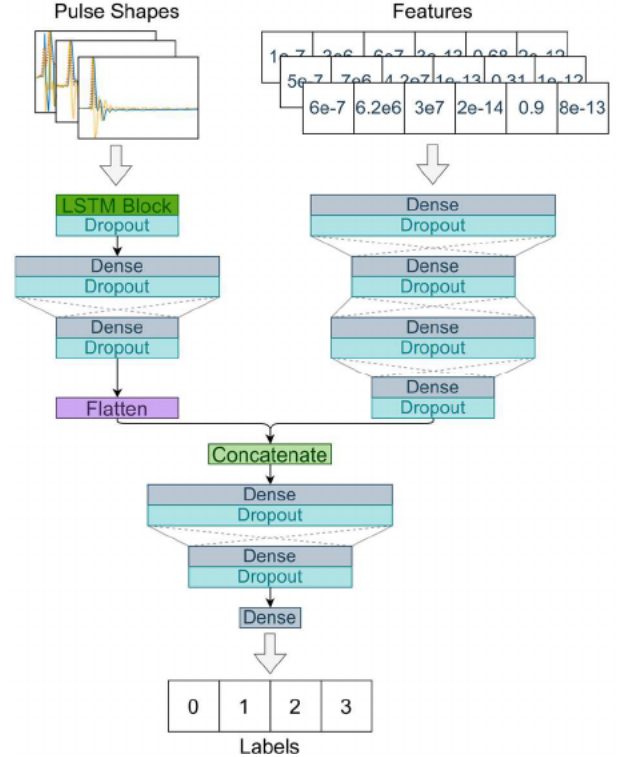


Fig. 14. MLP-induced LSTM schematic.

This model includes more hidden nodes as well as a more complicated structure and thus requires comparatively higher processing time.

3) Image Recognition Network

This approach includes a simplified version of the image recognition network proposed in [8], combined with a fully connected multilayer perceptron (Fig. 15).

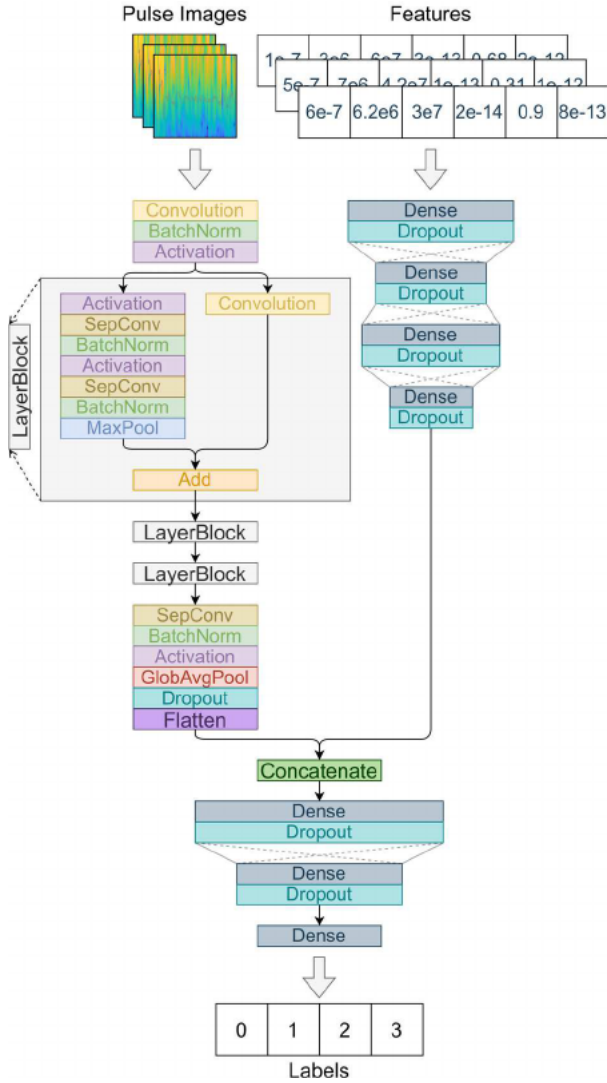


Fig. 15. Xception-based, MLP-induced image recognition schematic.

This network has the highest memory and computation requirements. Furthermore, image generation duration exceeds that of the pulse shape export roughly 20-fold.

IV. RESULTS

A. Training

Fig. 16 and Fig. 17 show the training histories of the different networks.

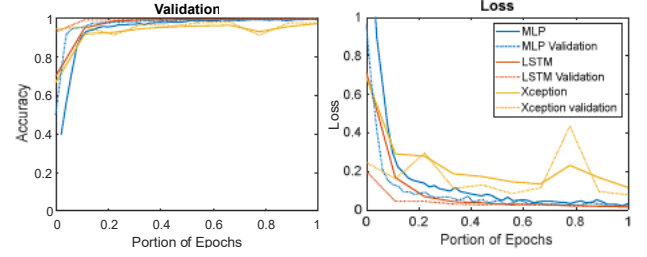


Fig. 16. Training histories.

The graphs show valid learning curves and acceptable accuracy for all networks. Especially the validation accuracy shows that all the approaches can classify data acquired from air- and polymer-based specimens. To evaluate their applicability to ceramics, various parameters are taken into consideration:

- In-class similarity
- Inter-class overlap
- Concordance of predictions using pulse shapes
- Concordance of predicted regarding expected PD sources
- Differentiability of classes compared to training data

B. Classification of Ceramic Measurement Data

To compare the networks regarding the first four parameters, Fig. 17 - 20 show PRPDs, T/W maps, and pulse shapes.

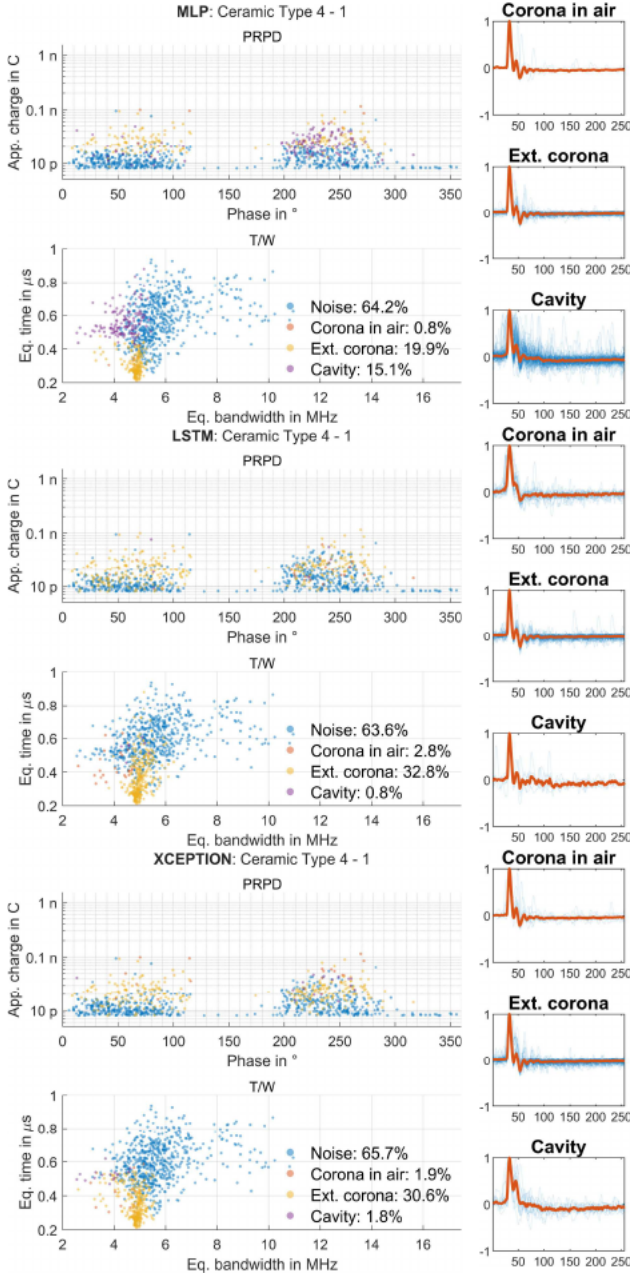


Fig. 17. PRPDs and T/W maps of Ceramic Type 4 - 1 measurements, labeled by the three different networks.

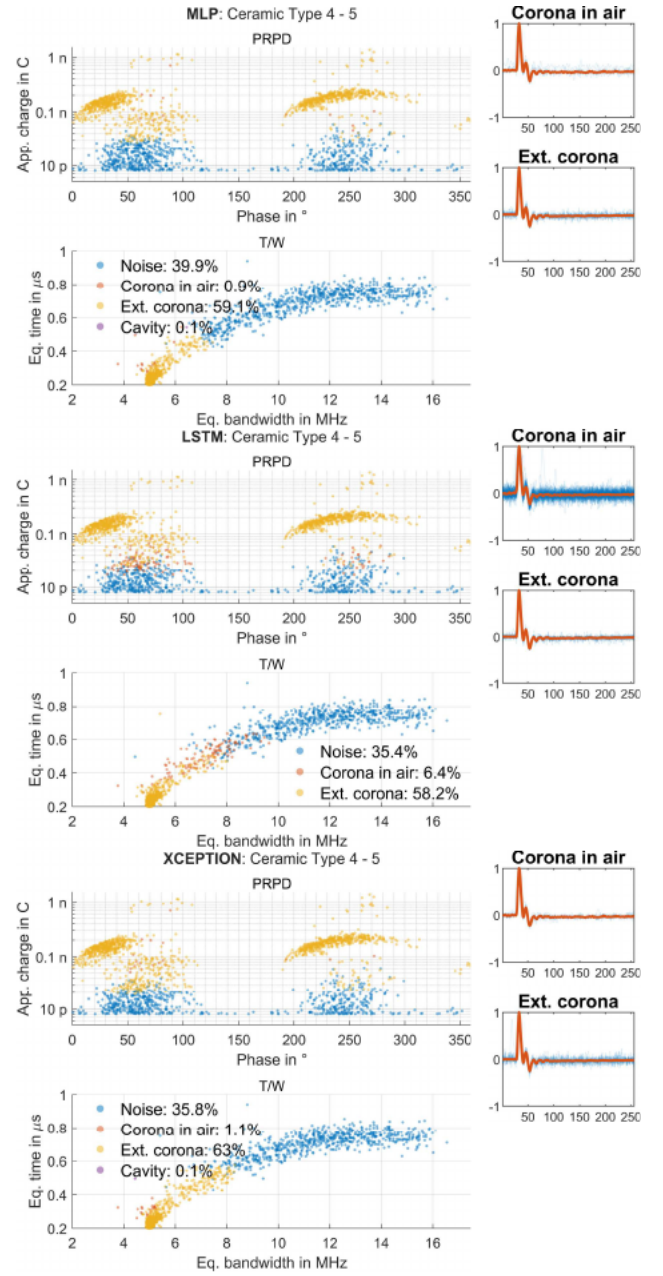


Fig. 18. PRPDs and T/W maps of Ceramic Type 4 - 5 measurements, labeled by the three different networks.

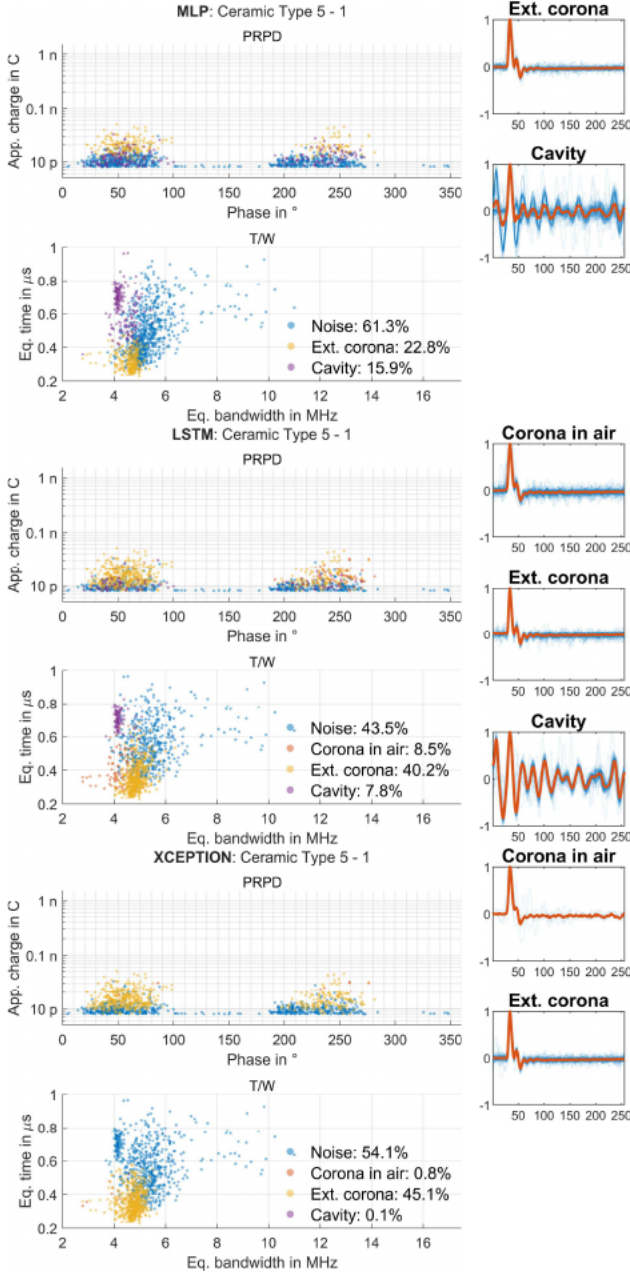


Fig. 19. PRPDs and T/W maps of Ceramic Type 5 - 1 measurements, labeled by the three different networks.

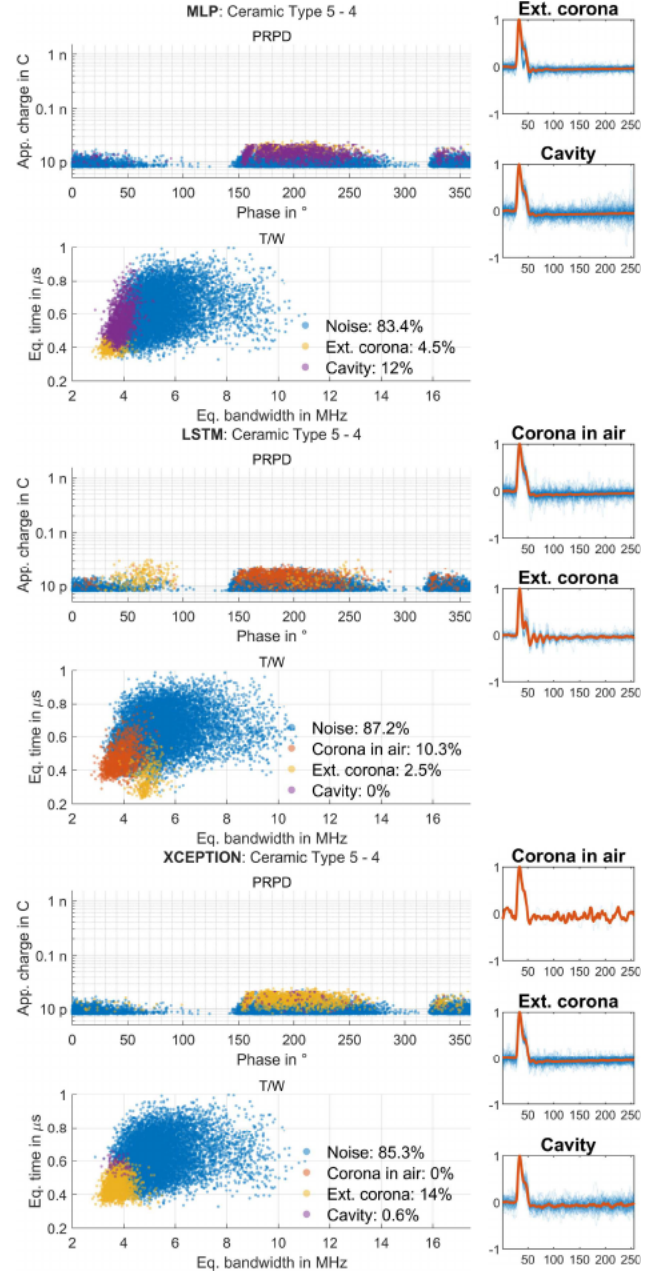


Fig. 20. PRPDs and T/W maps of Ceramic Type 5 - 4 measurements, labeled by the three different networks.

This overview demonstrates that considering solely features is not sufficient. The MLP figures show this by strongly scattered clusters as well as by pulses clearly recognizable as misassigned based on their pulse shapes (e.g. Fig. 17). The two pulse shapes-considering networks show a higher susceptibility to misclassification of individual pulses as seen by sub-percentage sample counts. Since the Xception-based network misclassifies some visible clusters as noise (e.g. Fig. 19) whilst also requiring significantly more computing power, the LSTM-based network seems to be most suitable regarding the first four parameters.

C. Evaluation of Group Separation Based on Pulse Sequence Analysis

To examine the LSTM's differentiability of the detected classes compared to training data, apparent charge PSA is performed on the data, shown in Fig. 21 to Fig. 23.

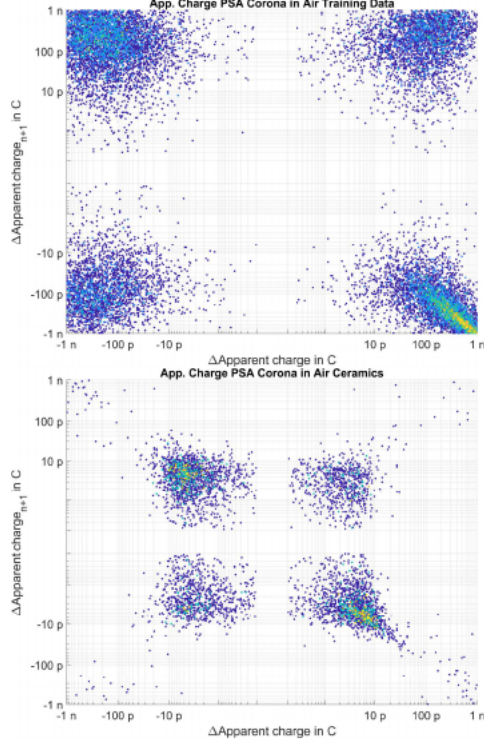


Fig. 21. Apparent charge PSA of accumulated auto-labeled corona in air data acquired from training data (top) and ceramics (bottom).

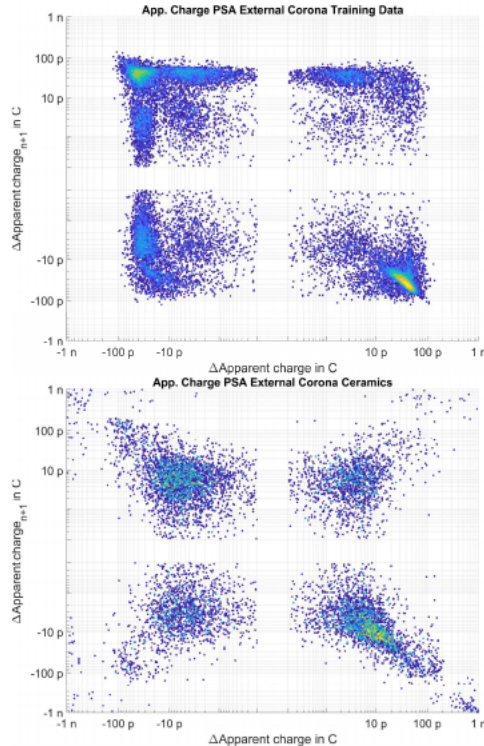


Fig. 22. Apparent charge PSA of accumulated auto-labeled external corona data acquired from training data (top) and ceramics (bottom).

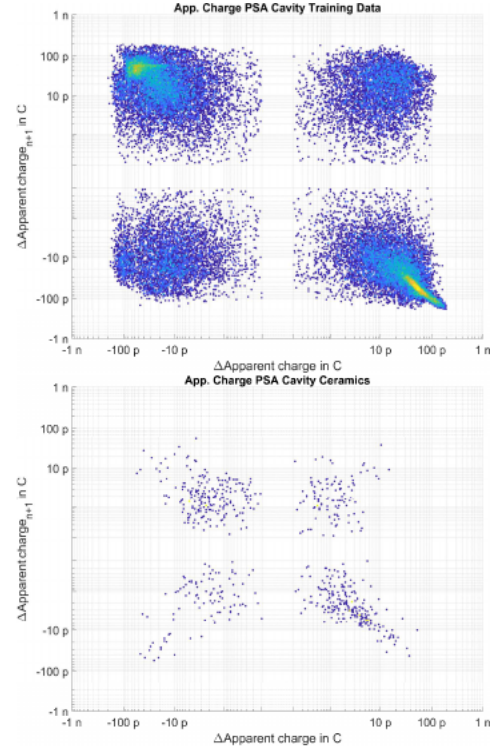


Fig. 23. Apparent charge PSA of accumulated auto-labeled cavity data acquired from training data (top) and ceramics (bottom).

Although the shapes of the LSTM-based corona and cavity clusters are roughly similar to those of the training data, significant differences are apparent. Visually, this can be explained by the differences in the number of data points. For the density-independent differences, two explanations are suggested:

- Misclassification
- Material-dependent partial discharge repetition behavior of identical discharge sources

V. DISCUSSION AND FUTURE WORK

Since it is evident in the LSTM-classified pulse shapes that at least corona and cavity discharges are correctly detected, fundamental misclassification can be ruled out. It is conceivable that, due to the lack of manual differentiability between external corona and internal glide discharges (if present), this differentiation is also impossible for the network. This can be prevented in the future by fabricating and measuring polymer-based substrates with assured glide discharge occurrence. To be able to investigate the differences in PD behavior between polymers and ceramics given the same discharge types in more detail, defined ceramics measurement samples are needed. However, with this constraint, several key points were demonstrated:

- The developed synchronization solution enables targeted raw data extraction using a variety of measurement devices not designed for interoperability
- The calculated features are suitable for a deeper PD measurement data analysis

- The demonstrated approach allows for knowledge transfer from air- and polymer-based measurements to ceramics
- The developed LSTM-based artificial neural network is able to distinguish PD shapes and thereby detect different PD sources with moderate computational resource requirements

This allows the demonstrated toolchain to be trained and used on other test beds or for different substrates such as complete power electronics assemblies. Consequently, new possibilities in defect detection or early failure detection that were previously impossible due to the demonstrated superimpositions and abundance of data are opened up. Work is also underway to develop an FPGA-based measuring device that performs both feature extraction and LSTM classification directly at the point of measurement, allowing each charge-time sample to be immediately labeled for advanced defect detection.

ACKNOWLEDGMENT

Research was done within the project „PROGNET - IDA / Datengenerierung und Messtechnik“ funded by the German Federal Ministry for Economic Affairs and Climate Action (grant number 16KN054235).

REFERENCES

- [1] A. Gemant, W. Philippoff, „Die Funkenstrecke mit Vorkondensator.“, „Z. techn. Phys.“, Berlin, Vol. 13, 1932, pp. 425-430.
- [2] W. Hauschild, E. Lemke, “High-Voltage Test and Measuring Techniques”, Springer Vieweg Berlin Heidelberg, Vol. 1, 2014, pp. 157-162.
- [3] International Electrotechnical Commission, IEC 60270, “High-voltage Test Techniques: Partial Discharge Measurements”, International Electrotechnical Commission, Vol. 3, 2014.
- [4] F. H. Kreuger, E. Gulski, A. Krivda, “Classification of Partial Discharges”, IEEE Trans. on EI, 28, (1993), 917-31.
- [5] R. Patsch, D. Benzerouk, “Characterization of Partial Discharge Processes- What Parameters work best?”, ICSD'04, Toulouse, France, (2004), 636-9.
- [6] A. Cavallini, G. C. Montanari, D. Fabiani, L. Testa, “Advanced technique for partial discharge detection and analysis in power cables”, Int. Conf. on Condition Monitoring & Diagnostic Engineering Management of Power Station / Substation Equipment, 2009.
- [7] A. R. Mor, L. C. Heredita, F. A. Muñoz, “Effect of acquisition parameters on equivalent time and equivalent bandwidth algorithms for partial discharge clustering”, International Journal of Electrical Power & Energy Systems, Volume 88, 2017, pp. 141-149.
- [8] F. Chollet, “Xception: Deep Learning with Depthwise Separable Convolutions,” in 2017 IEEE Conference on Computer Vision and Pattern Recognition (CVPR), Honolulu, HI, USA, 2017 pp. 1800-1807